Behavior of H_2^+ and H_2 in strong laser fields simulated by fermion molecular dynamics

K. J. LaGattuta
Los Alamos National Laboratory, MS-B259, Los Alamos, New Mexico 87545, USA
(Received 6 January 2006; revised manuscript received 15 February 2006; published 7 April 2006)

In this paper we describe an application of fermion molecular dynamics to the simulation of the behavior of H_2^+ and H_2 immersed in a strong laser field. The laser field consists of a single short pulse of linearly polarized long wavelength radiation; viz., $t_{pulse} \sim 100$ fs, $\lambda = 758$ nm, and $10^{13} \leqslant I_0 < 10^{14}$ W/cm^2. Results are compared with data from recent laboratory measurements.

DOI: 10.1103/PhysRevA.73.043404 PACS number(s): 33.80.Rv, 31.15.Qg

I. BACKGROUND

Established methods for describing atoms, or molecules, immersed in strong laser fields begin with an application of the time-dependent Schrodinger equation (or the Dirac equation if $I_0 > 10^{19}$ W/cm^2) to the modeling of a single electron, bound initially to an individual ion, and evolving under the influence of a short pulse laser field [1]. Description of such two-dimensional systems (for linearly polarized lasers, and initial *s*-wave bound states), or three-dimensional systems (for circularly polarized lasers and initial *s*-wave bound states, or for linearly polarized lasers and initial non-*s*-wave bound states) is easily accessible to computation using modern coumputers.

Description of the time-dependent motion of a single electron, bound initially by a two-centered potential, and interacting with a laser pulse is no more complicated, although this is usually a three-dimensional problem even for a linearly polarized laser; e.g., the H_2^+ molecular ion. Indeed, published accounts of work of this sort are now common. A correct description of the motion of the nuclei is more difficult, although progress has been made in this domain as well [2,3].

For systems of two electrons initially bound, direct application of the time-dependent Schrodinger equation (TDSE) is still somewhat problematic, although much progress has been made. So, for example, the H_2 system has been treated with considerable success [4]. For three or more electrons, much work remains to be done, as rigorous methods still do not allow, generally, for a satisfactory description of the large number of possible processes.

It was with these limitations, presented by the so-called rigorous methods, in mind that we first proposed, many years ago, to apply the fermion molecular dynamics (FMD) approach to simulations of the behavior of multielectron ionic states immersed in strong laser fields. Our first simulation, performed for He atoms, was quite successful [5].

An outcome of that work was our validation of a now well-known conjecture [6] concerning the origin of the plateau structure in experimentally determined distributions of double-ionization probability versus laser intensity, for two electron ions interacting with short pulse, long wavelength, laser radiation. Specifically, it was alleged that this structure originated in an overlap of the probability distributions for ordinary sequential double ionization, at relatively large laser intensities, and a new process dubbed nonsequential double ionization (NSDI), at lower laser intensities. The NSDI process was thought [6] to arise through a recollision of the first electron to be photoionized with the surviving one-electron ion, during which a collisional ionization of this residual electron occurred.

FMD simulations for an argon atom interacting with a strong laser field then ensued [7]. In this work, nonsequential multielectron ionization (NSMI) was observed. We found that the NSMI process was also driven by recollision. In particular, it was observed that the outermost electron in neutral argon, following its photoionization, could be driven back into the 1^+ ion. One or more electrons might then be released in a collisional ionization process. Moreover, it was noted that the probability distributions for multielectron ionization showed more pronounced plateau structures, generally, than the corresponding distributions for double ionization.

Lately, there has been a renewed interest in the application of both the TDSE [8,9], as well as quasiclassical methods, to the description of the interaction of bound electronic systems with intense laser fields. The quasiclassical methods recently employed [10] to simulate atomic NSDI bear some resemblance to FMD.

Therefore, inspired by this changing context, and in the light of newer laboratory measurements made for H_2^+ and H_2 interacting with strong laser fields [11–15], we thought it worthwhile to apply the FMD method to simulations of the behaviors of these more challenging systems. Just as we have made a past application of the FMD method to systems for which more rigorous methods had previously also been applied, or for systems where only experimental measurements had been reported, so we intend to use these latest simulations as a further test of the reliability of FMD, as applied to a broad spectrum of problems in atomic and molecular physics. It will also be of interest to search for evidence of NSDI in these systems. In fact, the presence of this phenomenon has recently been deduced from experiments performed on the N_2 molecule [16].

The FMD molecular models which we employ were developed in part by Cohen [17] for molecular dynamics applications. They contain features which lead to accurate FMD calculations, for both H_2^+ and H_2, of the ground state electronic energies vs internuclear separation R, for almost all values of R. These models are slightly more elaborate than

those familiar from past FMD work. Thus, at the cost of introducing one additional FMD potential for H_2^+, and two additional FMD potentials for H_2, the molecular model for these systems is very much improved. An accurate formulation of the electronic energy vs R is expected to be critical for calculations of the photodissociation and photoionization probabilities of molecules.

II. SIMULATING H_2^+ INTERACTIONS WITH STRONG LASER FIELDS BY FMD

We have used the method of fermion molecular dynamics (FMD) [18–21] to simulate the behavior of the hydrogen molecular ion H_2^+, interacting with a short pulse of high intensity, long wavelength, laser radiation.

The simulations were performed by means of standard FMD procedures, which are by now well-established, and the limitations of which are rather well-understood. We summarize here the simplest of the equations of FMD, using the example of atomic systems, and omitting any mention of the complications introduced by electron exchange. For the systems which we are considering in this paper, exchange does not enter.

In simplest form, the FMD equations form a coupled set of Hamilton's equations for the charged particles of interest:

$$d\vec{r}_i/dt = \nabla_{\vec{p}_i} H, \tag{1}$$

$$d\vec{p}_i/dt = -\nabla_{\vec{r}_i} H. \tag{2}$$

The Hamiltonian H contains the conventional bare Coulomb potentials, a term coupling the charges to an external electric field $\vec{E}(t)$, and a set of momentum dependent potentials V_H, acting between electrons and nuclei, which simulate the effect of the Heisenberg uncertainty principle:

$$H = \Sigma_i [p_i^2/2m_i + q_i e\vec{r}_i \cdot \vec{E}(t) + q_i \Sigma_{j<i}(q_j e^2/r_{ij}) + \Sigma_{j<i} V_H(r_{ij}, p_{ij})] \tag{3}$$

in natural units, where $q=1$ for protons and $q=-1$ for electrons. The potential V_H is given by

$$V_H = [A_H/r_{ij}^2]\exp(-B_H r_{ij}^4 p_{ij}^4), \tag{4}$$

where A_H and B_H are positive real constants, chosen to produce accurate values of the ground state (g.s.) energy and the average g.s. orbital radius. The relative momenta are the usual

$$\vec{p}_{ij} = [m_j\vec{p}_i - m_i\vec{p}_j]/[m_i + m_j]. \tag{5}$$

The FMD equations aim to replace, in an approximate fashion, the precise Bohmian equations of quantum mechanics for the velocity fields $\vec{v}_i(\vec{r}_i, t)$ of the interacting particles. These velocity fields depend critically upon the so-called quantum potentials [18], which must be computed at every time step, and do not generally have a fixed algebraic form. In particular, in FMD the delocalization of $\vec{v}_i$ in space is replaced by the ansatz of a momentum dependence, and the quantum potential is replaced by the ansatz of a fixed algebraic form V_H. For more information on the FMD method, consult Refs. [5,18,19].

Now, in contrast to the approach outlined above, and in Ref. [5], an additional FMD potential is invoked to facilitate simulation of the H_2^+ problem. This additional potential allows for an accurate rendering of the electronic ground state $(1s\sigma_g)$ energy vs internuclear separation R, for almost all values of R [17]. In contrast to the recent work of another theory group [3], we do not reproduce the electronic energy vs R curve of the first excited state $(2p\sigma_u)$; i.e., since the excited electronic states are always arrayed into a continuum, in the present formulation of FMD.

The additional FMD potential, peculiar to H_2^+, is

$$V_{H_2^+} = [A_{H_2^+}/r_{23}^2]\exp(-B_{H_2^+} r_{23,1}^4 p_{23,1}^4), \tag{6}$$

where $r_{23,e}$ is the difference between the diproton center-of-mass coordinate (protons labeled 2 and 3) and the electron coordinate (electron labeled 1).

The initial values of the electron coordinates and momenta, and the proton coordinates were adapted from Ref. [17], where the values quoted were specific for the case of fixed, or infinite mass, nuclei. For the case of moving nuclei, and after adjustments ensuring that the total momentum of the molecular ion, and the total angular momentum about its center-of-mass, are both zero, these intial values become: $x(0)=0.6572$ a.u., $y(0)=0.0$, and $z(0)=0.5095$ a.u., for the electron coordinates, and $p_x(0)=1.0362$ a.u., $p_y(0)=p_z(0)=0.0$, for the electron momenta. Also, $X_1(0)=X_2(0)=Y_1(0)=Y_2(0)=0.0$, $Z_1(0)=1.1614$ a.u., $Z_2(0)=-Z_1(0)$, are the coordinates of protons 1 and 2, and $P_{1x}(0)=-0.7454$ a.u., $P_{2x}(0)=-0.2908$ a.u., $P_{1y}(0)=P_{2y}(0)=P_{1z}(0)=P_{2z}(0)=0.0$, are their corresponding momenta.

For this choice of coordinates and momenta, all three particles are at rest, and the total force on each particle is zero. This condition of complete stasis is a feature of any FMD ground state.

Then, in order to include as a part of the initial condition that state of rovibrational excitation which might be encountered in an actual laboratory measurement, we imparted rovibrational motion to the two protons, corresponding to an arbitrarily chosen temperature of 600 °C, or 0.07 eV; i.e., a total vibrational energy of 0.07 eV and a total rotational energy of 0.07 eV was included as a part of the initial conditions.

The laser was taken to be linearly polarized, with frequency $\omega=0.060$ a.u. ($\lambda=758$ nm) and, in most cases, pulse length $t_{pulse}=4300$ a.u. (100 fs). The pulse had a simple sine function turn-on and turn-off transient, each of duration 150 a.u., while the main portion of the pulse was of constant amplitude, and lasted for 4000 a.u. The initial angle between the internuclear axis and the laser polarization direction was selected randomly.

For a range of peak laser intensities, data describing all of the possible final states was accumulated; i.e., the states of (a) H_2^+ (elastic and quasielastic processes); (b) $H^* + p^+$ (photodissociation, where the asterisk indicates a possible excited state of the residual atom); and (c) $e^- + 2p^+$ (photodissociative ionization). In Fig. 1, we plot values of the logarithm of

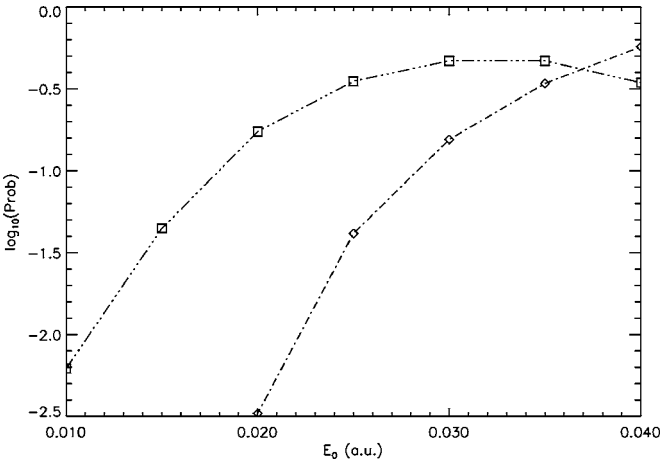

FIG. 1. Transition probabilities vs E_0 for $H_2^+\gamma's \rightarrow H^* + p^+$ (squares); $e^- + 2p^+$ (diamonds); with $\omega = 0.060$ a.u. ($\lambda = 758$ nm), and $t_{pulse} = 4300$ a.u. (100 fs).

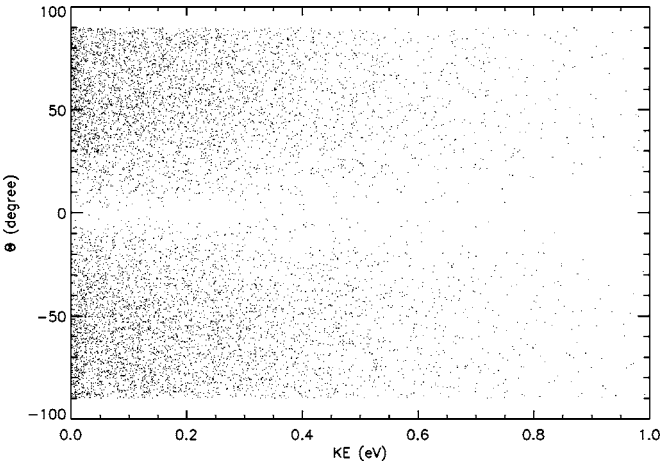

FIG. 2. For photodissociation of H_2^+: distribution of fragment emission angles relative to the laser electric field vector vs fragment kinetic energies; data for H and p^+ are plotted together; with $E_0 = 0.035$ a.u. ($I_0 = 4.30 \times 10^{13}$ W/cm^2), $\omega = 0.060$ a.u. ($\lambda = 758$ nm), and $t_{pulse} = 4300$ a.u. (100 fs). The difference in the distributions for H and p^+ is readily apparent only after summing over energies; see Fig. 3. KE denotes kinetic energy.

the transition probability vs the laser peak electric field strength, in atomic units (a.u.). The laser intensity is related to the peak electric field strength by $I_0(\mathrm{W/cm^2}) = 3.51 \times 10^{16} E_0^2(\mathrm{a.u.})$.

In the region of E_0 values considered here, the probability of photodissociation was usually large relative to the probability of photoionization. The reason seems to be that the electric field strength is too small to induce direct ionization of the molecular ion, with any appreciable probability. An estimate of the threshold electric field strength for over-the-barrier ionization (OBI) of the molecular ion is $E_0 = 0.044$ a.u., which is above the range of values employed in these simulations; i.e., for zero initial vibrational energy. See the Appendix for further information.

However, it is relevant to recall that FMD calculations perforce neglect tunneling ionization. Therefore, in the region of E_0 values which we are working, it is reasonable to believe that tunneling ionization may be important, our observed predominance of photodissociation over photoionization may be, to some extent, artifactual. (Allowance can be made for the inherently quantum mechanical process of tunneling, within FMD calculations, at least for one electron system [22]. We have not attempted to employ such methods here.)

It is also true that photoionization in FMD can occur for field strengths below the OBI threshold by a purely classical process. This begins with a continuous excitation of the bound electron, followed by photoionization from an unphysical continuum of low-lying excited states; i.e., since bound excited electronic levels are not discrete in FMD. The continuous excitation of the bound electron is unrelated to power broadening, and ionization below the OBI threshold, in FMD, is distinct from tunneling ionization. This is clearly a defect of the FMD method. Even though it is true that, in nature, for bound systems of two or more electrons, correlation effects can increase the number of low-lying excited states [8], still these states remain discrete, relatively few in number, and well-separated from the ground state; see the Discussion section.

With these caveats firmly in mind, we report our finding that the ionization of the molecular ion proceeds, usually, by a two-step process: a dissociating state of H_2^+, accompanied by a small amount of electronic excitation of the residual hydrogen atom (H^*), is followed by photoionization of the excited atom. The second step occurs, typically, at a value of the diproton spacing in the range 3 a.u. $< R <$ 5 a.u. For simplicity of notation the asterisk, denoting a low-lying excitation of atomic hydrogen, is omitted from the following presentation.

For photodissociation, we found that the angular distribution of H was approximately isotropic with respect to the laser electric field, albeit with a small bias toward emission in a direction *normal* to the field. This bias was observed to increase as the laser pulse length was decreased; i.e., for pulse lengths such that $t_{pulse} < 100$ fs. At the same time, the p^+ angular distribution showed a spike of probability in the direction *parallel* to the laser field. The sharpness of this spike also tended to increase as the laser pulse length was decreased; see Figs. 2–4. A small spike also emerged along the forward direction in the angular distribution of emitted H, as the pulse length was decreased; see Fig. 4.

These aspects of the FMD simulation, for H_2^+ targets, are in only fair accord with recent laboratory measurements; compare Figs. 2–4 with data contained in Refs. [11–13]. Those laboratory measurements show that fragments are emitted, preferentially, along the laser electric field. However, the conditions employed in those experiments are usually rather different from ours. For example, in Fig. 1(a) of Ref. [11] the pulse length was 575 fs, and in Fig. 1(b) the laser intensity was 1.5×10^{14} W/cm^2; in Fig. 1 of Ref. [12] the laser intensity was 1×10^{15} W/cm^2; and in Fig. 2 of Ref. [13] the laser intensity was 2.4×10^{14} W/cm^2. Longer laser pulse lengths and larger laser intensities would both be expected to lead to greater alignment of fragments with the laser field.

The measurements of Ref. [13] also show a sharp spike of probability in the laser field direction when $t_{pulse} = 45$ fs, but

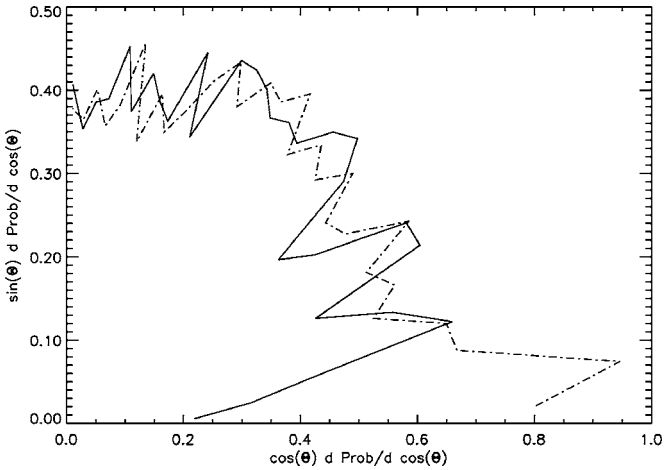

FIG. 3. For photodissociation of H_2^+: distribution of fragment emission angles, relative to the laser electric field (x axis); data for H (solid curve) and p^+ (dash-dot curve) plotted separately after summing over energies; the magnitude of a vector drawn from the origin to a point on the figure equals the differential emission probability $d\,\mathrm{Prob}/d\cos(\Theta)$, at the angle Θ subtended by that vector and the x axis; for the data of Fig. 2.

not when $t_{pulse}=135$ fs; see their Figs. 2 and 3. This is in accord with the results of our simulations.

For high energies of the emitted fragments our simulations show that H and p^+ tend to travel in nearly opposite directions; i.e., for single events, and when the kinetic energy is such that $E_{kin}>1$ eV. However, for $E_{kin}<0.01$ eV, H and p^+ tended to move at nearly right angles to each other.

For photoionization, protons emitted during the corresponding Coulomb explosion process were strongly correlated, always emerging in essentially opposite directions. The single proton angular distribution was, however, biased toward shallow angles, with a peak occurring near 30°, relative to the laser electric field; see Figs. 5 and 6. As was the case for photodissociation, decreasing the laser pulse length from $t_{pulse}=100$ to 50 fs resulted in a proton angular distribution skewed more toward the normal. But, for the shorter laser

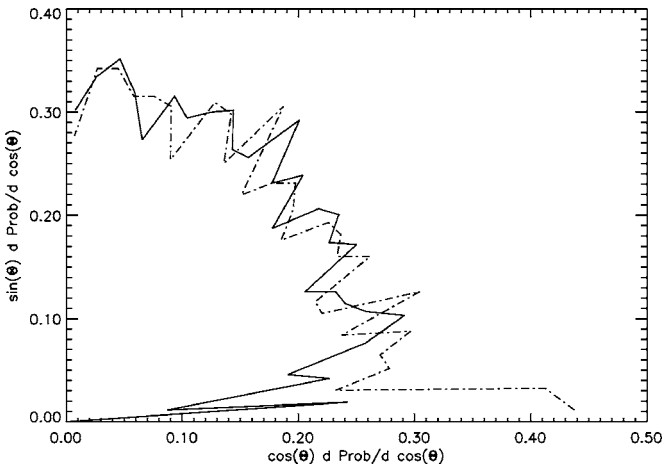

FIG. 4. For photodissociation of H_2^+: with $E_0=0.055$ a.u. ($I_0=1.06\times10^{14}$ W/cm^2), $\omega=0.060$ a.u. ($\lambda=758$ nm), and $t_{pulse}=2300$ a.u. (50 fs).

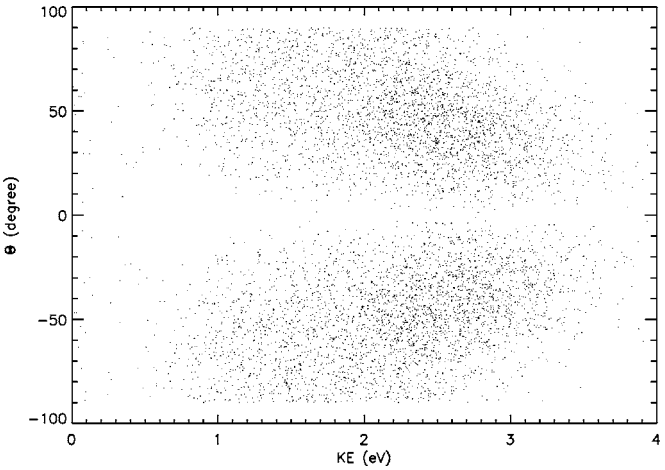

FIG. 5. For photoionization of H_2^+: distribution of p^+ emission angles relative to the laser electric field vector vs p^+ kinetic energies; $E_0=0.035$a.u. ($I_0=4.30\times10^{13}$ W/cm^2), $\omega=0.060$ a.u. ($\lambda=758$ nm), and $t_{pulse}=4300$ a.u. (100 fs).

pulse length, a sharp peak in the forward direction also appeared; see Fig. 7.

Recent laboratory measurements show a distribution of proton emission angles peaked in the forward direction for photoionization; see Ref. [12]. The measurements of Ref. [13] show an angular distribution which is even more sharply confined to the forward direction. Our simulations exhibit a behavior which is somewhat reminiscient of these measurements.

Generally, we observed that electrons emitted during photoionization traveled preferentially along the laser electric field, with the highest energy electrons showing the greatest degree of alignment with the field. Indeed, the tendency for particles with the largest kinetic energies to emerge in closest alignment with the laser field was a ubiquitous feature of our simulations, and occurred as well for proton angular distributions.

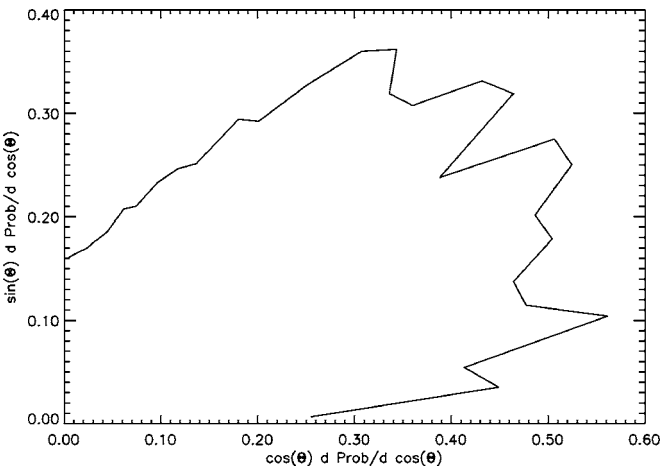

FIG. 6. For photoionization of H_2^+: distribution of p^+ emission angles, relative to the laser electric field (x axis), after summing over energies; plotted such that the magnitude of a vector drawn from the origin to a point on the figure equals the differential emission probability $d\,\mathrm{Prob}/d\cos(\Theta)$, at the angle Θ subtended by that vector and the x axis; for the data of Fig. 5.

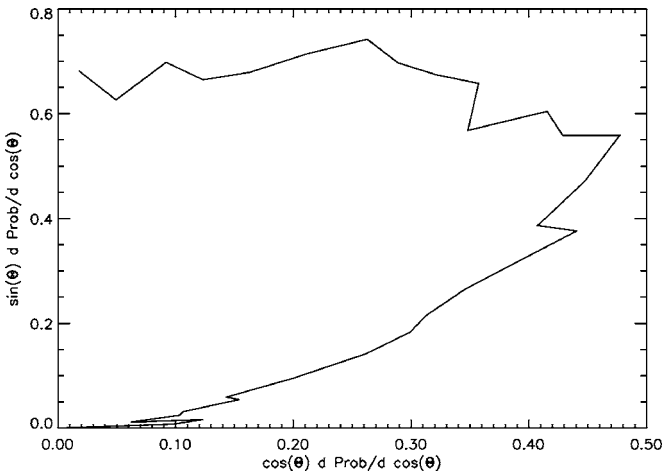

FIG. 7. For photoionization of H_2^+: conditions as in Fig. 4.

We have also observed these behaviors directly by tracking the time-dependent coordinates of all three charged particles, for a large number of independent trials. Concerning these studies, several remarks are in order.

During trials for which H_2^+ neither dissociated nor ionized, the diproton vibrated regularly with a measured period $T_{vib} \approx 1100$ a.u. (27 fs), implying a total vibrational energy of $\omega_{vib} = 2\pi / T_{vib} \approx 0.0057$ a.u. (0.155 eV). The corresponding time-averaged vibrational kinetic energy was determined to be $\langle (E_{kin})_{vib} \rangle \approx 0.0029$ a.u. (0.079 eV).

In the vast majority of photoionization events observed, the electron was emitted from the vicinity of the dissociating diproton abruptly, and when 3 a.u. $< R < 5$ a.u., as already mentioned. It is worth pointing out, however, that such cases occurred only when $\vec{R}$ was nearly perpendicular to the laser electric field; e.g., for $70° < \theta < 110°$, where θ is the angle between $\vec{R}$ and $\vec{E}_0$. But, in those rare events in which photoionization occurred while the diproton was aligned nearly along the laser field, ionization could not be said to be complete until much larger values of R had been attained. This was because, in the nearly parallel geometry, the laser field drove the electron into a series of repeated collisions with the dissociating diproton. A similar explanation has been offered recently to account for behaviors observed during the photoionization of N_2 [16].

The fact that the ground state of H_2^+, as described in FMD, has a permanent electric dipole moment is a defect of the method; see the initial values of the particle coordinates, which appeared earlier in this section. However, for a laser frequency of $\omega = 0.060$ a.u., and for the range of laser peak electric field strengths of interest here, the molecular ion does not have sufficient time to undergo appreciable alignment with the oscillating laser electric field, before the field reverses sign. We estimate that the amplitude of the oscillation in orientation of the internuclear axis, relative to the laser electric field, due to the erroneous assignment of a permanent dipole moment to the molecular ion, is no more than 5°.

It is also worth pointing out that the dynamically *induced* electric dipole moment was determined in these calculations to be much smaller, typically, than the erroneous permanent dipole, and played no essential role in the outcome of any particular simulation. Finally, rotational motion imparted to the molecular ion, as a part of its initial conditions, was such that the internuclear axis rotated freely through an angle of approximately 180° during the 100 fs long laser pulse. Thus change in the orientation of the internuclear axis relative to the laser electric field appeared to be due almost entirely to the initial conditions. Alignment along the laser electric field of the erroneous permanent dipole moment, or of the dynamically induced dipole moment, was not observed, and cannot be said to have played an essential role in the fragmentation of H_2^+ observed in these calculations.

III. SIMULATING H_2 INTERACTIONS WITH STRONG LASER FIELDS BY FMD

In this section, we present results obtained from FMD simulations describing the behavior of molecules of hydrogen H_2, interacting with a short pulse of high intensity, long wavelength, laser radiation. Methods employed were identical to those described in the previous section. FMD potentials peculiar to H_2^+ were included, one for each electron; see Eq. (6). In addition, an FMD potential peculiar to H_2 was included:

$$V_{H_2} = [A_{H_2}/r_{34}^2] \exp(-B_{H_2} r_{12}^4 p_{12}^4), \tag{7}$$

where now the electrons are labeled 1 and 2, and the protons are labeled 3 and 4. With this choice, we are able to accurately reproduce the known values of the ground state electronic energy vs internuclear distance, R [17].

As in the previous section, the initial values of the electron coordinates and momenta, and the proton coordinates were adapted from previous work [17], in which the values quoted were specific for the case of fixed, or infinite mass, nuclei. For the case of moving nuclei, and after adjustments ensuring that the total angular momentum about its center-of-mass is zero, these intial values become: $x_1(0) = 0.8714$ a.u., $y_1(0) = 0.0$, $z_1(0) = 0.3283$ a.u., $x_2(0) = -x_1(0)$, $y_2(0) = -y_1(0)$, $z_2(0) = -z_1(0)$, for the coordinates of electrons 1 and 2, and $p_{1x}(0) = 1.0331$ a.u., $p_{2x}(0) = -p_{1x}(0)$, $p_{1y}(0) = p_{2y}(0) = p_{1z}(0) = p_{2z}(0) = 0.0$, for their momenta. Also, $X_1(0) = X_2(0) = Y_1(0) = Y_2(0) = 0.0$, $Z_1(0) = 0.6955$ a.u., $Z_2(0) = -Z_1(0)$, are the coordinates of protons 1 and 2, and $P_{1x}(0) = -0.4877$ a.u., $P_{2x}(0) = -P_{1x}(0)$, $P_{1y}(0) = P_{2y}(0) = P_{1z}(0) = P_{2z}(0) = 0.0$, are their corresponding momenta.

For this choice of coordinates and momenta, all four particles are at rest, and the total force on each particle is zero. As mentioned previously, this condition of complete stasis is a feature of the FMD ground state. In order to include as a part of the initial condition that state of rovibrational excitation which might be encountered in an actual experimental measurement, we imparted rovibrational motion to the two protons, corresponding to an arbitrarily chosen temperature of 600 °C.

Again, the laser was linearly polarized with frequency $\omega = 0.060$ a.u. ($\lambda = 758$ nm) and pulse length $t_{pulse} = 4300$ a.u. (100 fs). The pulse had a simple sine function turn-on and turn-off transient, each of duration 150 a.u., while the main

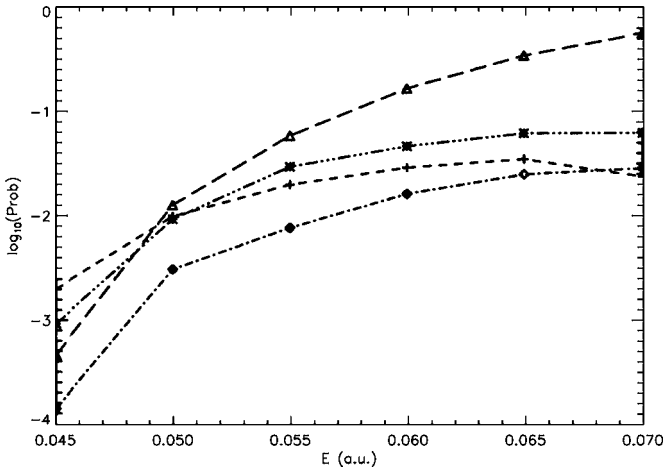

FIG. 8. Transition probabilities vs E_0 for $H_2+\gamma' s \rightarrow 2H$ (crosses); $H_2^+ + e^-$ (diamonds); $H^* + e^- + p^+$ (asterisks); $2e^- + 2p^+$ (triangles); all with $\omega = 0.060$ a.u. ($\lambda = 758$ nm), and $t_{pulse} = 4300$ a.u. (100 fs).

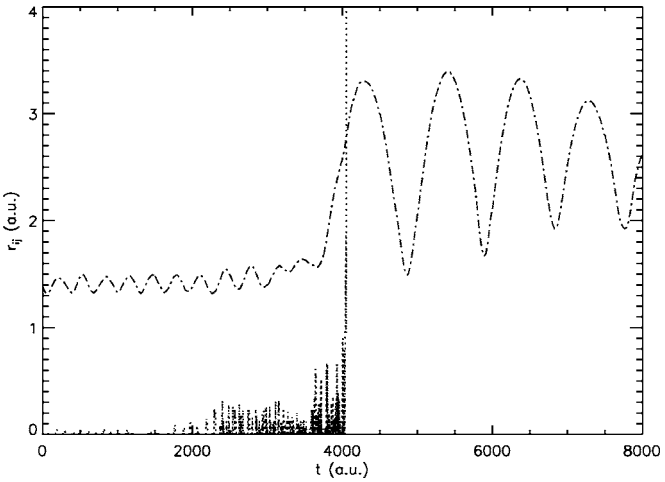

FIG. 9. Interparticle spacings r_{ij} vs time t for the process $H_2 + \gamma' s \rightarrow H_2^+ + e^-$, with $E_0 = 0.050$ a.u., $\omega = 0.060$ a.u., and $t_{pulse} = 4300$ a.u.; diproton spacing $r_{pp} \equiv R$ (dash-dot curve); electron-proton spacing r_{ep} for the ionizing electron, shifted toward zero by 1.0 a.u. for display purposes (dotted curve).

portion of the pulse was of constant amplitude, and lasted for 4000 a.u. The initial angle between the internuclear axis and the laser polarization direction was selected randomly.

Rationalizations of the detailed results displayed in Fig. 8 are, generally, more complex than those outlined for the molecular ion, in the preceding section. The region of field strengths $0.045 \text{ a.u.} < E_0 < 0.055$ a.u. is particularly interesting. In this region, the probabilities for photodissociative ionization (asterisks), for double photoionization (triangles), and for simple photodissociation (crosses), are all very similar. But the probability to form H_2^+ (diamonds) is from 5 to 10 times smaller.

We note that our observation of a relatively large probability for simple photodissociation is not in accord with the laboratory evidence [14,15]. However, the experimental situation is still not entirely clear; see the Discussion section.

The reason for these observed behaviors may be that, in this region of relatively low field strengths it is difficult to remove an electron from H_2 without having first excited sufficient vibrational motion to stretch the molecule beyond about twice its normal equilibrium internuclear spacing. Indeed, it is well known that it is much easier to ionize H_2 at low field strengths if the molecule is first elongated. But, once the molecule has been stretched beyond $R \approx 3.0$ a.u., it is unlikely that single ionization will be followed by a return to a stable state of H_2^+.

In those rare cases where H_2^+ does form successfully, during the photoionization of H_2, we observe that the amplitude of vibrational motion of the diproton Δz_{vibr} increases, while the frequency of vibrational motion ω_{vibr} decreases; i.e., such that $\omega_{vibr} \Delta z_{vibr} \approx \text{const}$; see Fig. 9. Consequently, no significant amount of energy is transferred to the diproton during photoionization. As is seen in Fig. 9, H_2^+ forms in the vicinity of $t = 4000$ a.u., just before the laser pulse turns off; i.e., for this particular case. After the pulse has ended, the molecular ion remains stable, although there is some residual electronic excitation. As is always the case in FMD, excited electronic states are not discrete.

Notice also that the values of E_0 employed in these simulations was generally greater than for H_2^+. We can begin to understand this difference based upon a purely classical model, which is described in the Appendix. There we estimate the value of the electric field strength needed to ionize H_2 by the over-the-barrier mechanism to be $E_{OBI} \approx 0.065$ a.u.

Similar to the results obtained in the previous section, fragmentation of the H_2 molecule, in a photodissociative or a photoionization process, has been observed to proceed usually through a 2H intermediate state. We have observed this mechanism directly by tracking the time-dependent coordinates of all four charged particles, for a large number of independent trials. For these cases, ionization has been observed to occur, typically, at a value of the diproton spacing in the range $3 \text{ a.u.} < R < 10$ a.u., with an average value of $R \approx 5.0$ a.u.; see Fig. 15.

There is no obvious evidence of the presence of NSDI in Fig. 8; i.e., the curve of double photoionization probability vs laser peak intensity (triangles) is smooth and uninflected over its entire range. However, the data here is probably too sparse to allow for a confident judgement. In particular, all orientations of the internuclear axis relative to the laser electric field direction have been included in Fig. 8. There is some good reason to suppose that only cases in which the internuclear axis remains parallel to the laser field can contribute strongly to NSDI in the molecule [16]; but, see the Discussion section for further information.

In contrast to the case of H_2^+, the FMD description of the ground state of H_2 shows no permanent electric dipole moment. Also, as for H_2^+ the dynamically *induced* electric dipole moment of H_2 was determined to be small, and to play no essential role in the outcome of any particular simulation. As before, rotational motion imparted to the molecule, as a part of its initial conditions, was such that the internuclear axis rotated freely through an angle of approximately 300° during the 100 fs long laser pulse (H_2 has a smaller equilibrium internuclear separation than H_2^+ and, hence, a smaller moment of inertia). Again, change in the orientation of the

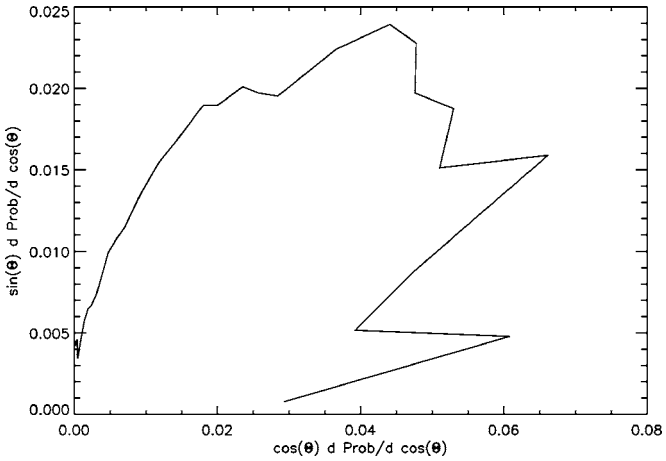

FIG. 10. For photodissociation of H_2: distribution of H emission angles, relative to the laser electric field (x axis), after summing over energies; plotted such that the length of a vector drawn from the origin to a point on the figure equals the differential emission probability $d\,\mathrm{Prob}/d\cos(\Theta)$, at the angle Θ subtended by that vector and the x axis; with $E_0=0.055$ a.u. ($I_0=1.06\times10^{14}$ W/cm^2), $\omega=0.060$ a.u. ($\lambda=758$ nm), and $t_{pulse}=4300$ a.u.. (100 fs).

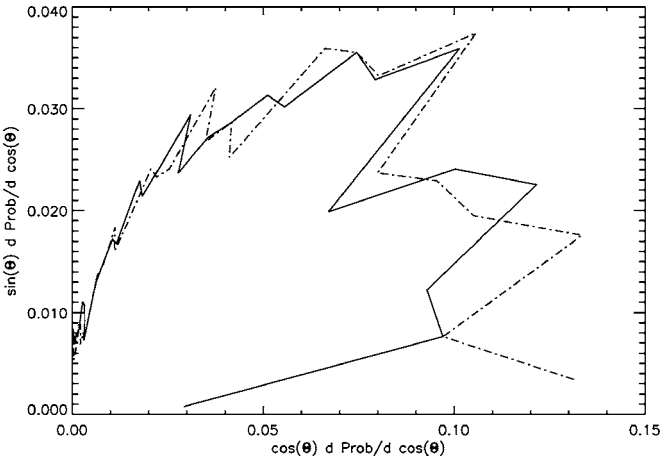

FIG. 11. For photodissociative ionization of H_2: distribution of heavy fragment emission angles, relative to the laser electric field (x axis); data for H (solid curve) and p^+ (dash-dot curve) plotted separately; for the conditions of Fig. 10.

internuclear axis relative to the laser electric field appeared to be due almost entirely to the initial conditions. Alignment along the laser electric field of the dynamically induced dipole moment was not observed, and cannot be said to have played an essential role in the fragmentation of H_2 observed in these calculations.

Fragment angular distributions obtained from the photodissociation and photoionization of H_2 are rather different from those obtained from H_2^+; see Figs. 11–13 and compare with the corresponding Figs. 3 and 6. In particular, we found that fragments formed during the breakup of H_2 show a larger probability of being emitted along the laser electric field, in agreement with earlier measurements [24]. Also, we found that fragments with larger values of the kinetic energy tended to be more closely aligned with the electric field than fragments with smaller values of the kinetic energy. This increased alignment was more evident for electrons than for protons, and more evident for protons than for hydrogen atoms; see Figs. 10–14. Sharp spikes of probability in the forward direction, seen for H_2^+ targets at short pulse lengths, were not observed for H_2. However, in the latter case, all of the angular distributions are displaced toward the forward direction. Thereby, the possible presence of small sharp features aligned with the laser field may be masked.

As mentioned earlier, the range of diproton spacings R over which ionization occurs was deduced from the observation of a limited number of individual particle trajectories to be 3 a.u.$<R<$10 a.u. This generalization is supported by the data of Fig. 12. After summing over Θ, we replot this data in Fig. 15 as the probability $d\,\mathrm{Prob}(R_{ioniz})/dR_{ioniz}$ vs R_{ioniz}, where $R_{ioniz}\equiv 1/[(E_{kin})_{p1}+(E_{kin})_{p2}]$ is the inverse of the sum of the kinetic energies of the emitted protons, and where we assume that a Coulomb explosion was initiated at $R=R_{ioniz}$.

Observations made of individual FMD particle trajectories also support the view that the H_2 molecule fragments least readily when it spends most of its time oriented nearly perpendicular to the laser electric field. Instead, fragmentation tends to occur on trajectories along which the molecule spends more time nearly aligned with the field. This is true for photodissociation, and becomes more obvious as the number of charged fragments in the final state increases. By contrast, fragmentation of H_2^+ was observed to occur most readily while the molecular ion was oriented perpendicular to the laser electric field. This was especially evident for shorter laser pulses and lower laser intensities.

IV. DISCUSSION

We refer again to a very recent publication describing laser induced breakup of H_2^+ [13]. The results of our simulations are in reasonable accord with the measurements reported in that paper, if allowance is made for the fact that the spatial profile of their laser pulse was such that a preponder-

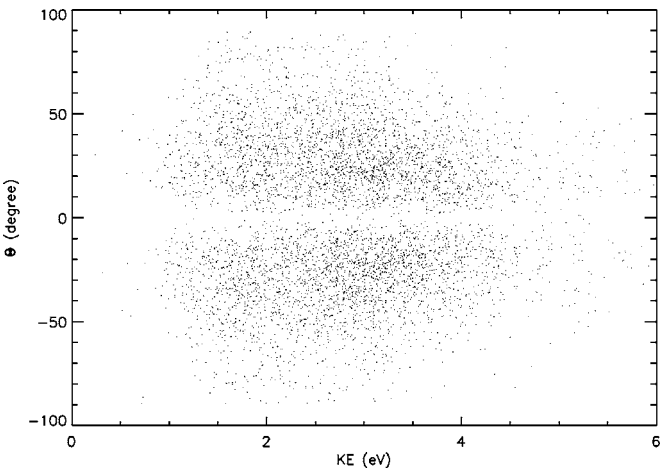

FIG. 12. For double photoionization of H_2: distribution of p^+ emission angles relative to the laser electric field vector vs p^+ kinetic energies; for the laser conditions of Fig. 10.

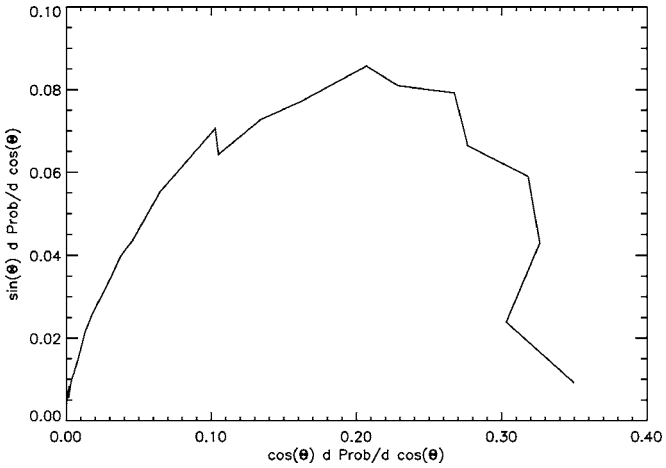

FIG. 13. For double photoionization of H_2: distribution of p^+ emission angles, relative to the laser electric field (x axis), after summing over energies; plotted such that the magnitude of a vector drawn from the origin to a point on the figure equals the differential emission probability $d\,\mathrm{Prob}/d\cos(\Theta)$, at the angle Θ subtended by that vector and the x axis; for the data of Fig. 12.

ance of interactions occurred at laser intensities lower than their tabulated peak intensity. For example, angular distributions of fragments emitted during photodissociation were similar to ours; i.e., as inferred from their so-called kinetic energy release (KER) plots. Also, a very sharp feature appeared in their KER data for protons emitted during photodissociation, with a kinetic energy of less than 0.5 eV, and for a laser pulse length of 45 fs. This feature was absent for a pulse length of 135 fs; see their Figs. 2(a) and 3(a), and compare with our Figs. 3 and 4.

Earlier in this paper we argued that, generally, one expects longer pulse lengths and higher laser peak intensities to lead to an increased alignment of emitted fragments with the laser field. However, we have also found that, at shorter pulse

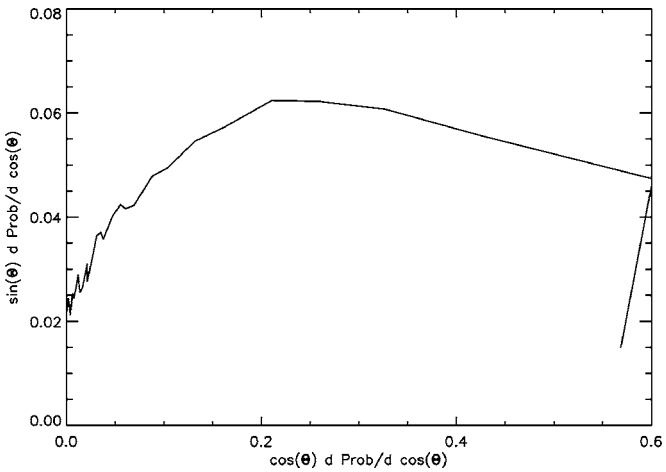

FIG. 14. For double photoionization of H_2: distribution of e^- emission angles, relative to the laser electric field (x axis), after summing over energies; plotted such that the magnitude of a vector drawn from the origin to a point on the figure equals the differential emission probability $d\,\mathrm{Prob}/d\cos(\Theta)$, at the angle Θ subtended by that vector and the x axis; for the laser conditions of Fig. 10.

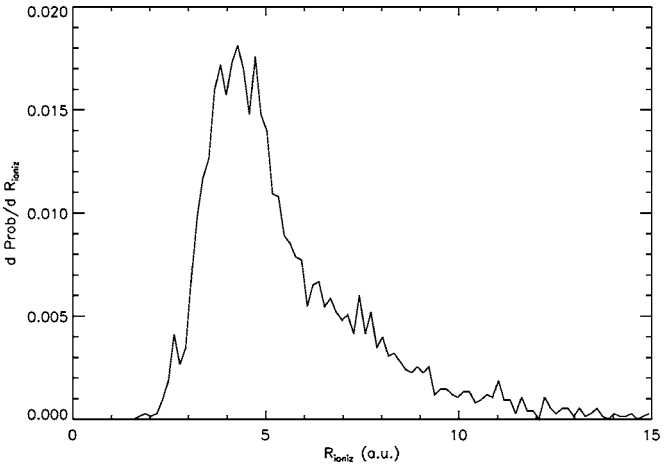

FIG. 15. For double photoionization of H_2: distribution of R_{ioniz} values as deduced from the data of Fig. 12 (summed over Θ), and such that $R_{ioniz}=1/[(E_{kin})_{p1}+(E_{kin})_{p2}]$, where $(E_{kin})_{pj}$ is the kinetic energy of the jth proton; see text.

lengths and lower laser peak intensities, a sharp structure appears in the forward direction, in agreement with the experiment [13] too. It may be that this sharp structure is also present at the longer pulse lengths and higher laser peak intensities, but is hidden by a greater skewing of the bulk of the emitted fragment probability distribution toward the forward direction. Possibly, there are two independent mechanisms at work here, each leading to the breakup of the target molecular ion. This is an area for furture work.

Differences between the results of our simulations and the experimental data [13] also exist. For example, for photoionization of H_2^+ the measured proton angular distribution was confined entirely to a sharp peak along the laser electric field direction, but, our simulations showed a significant probability of emission normal to the field; compare Fig. 3(c) of Ref. [13] with our Fig. 7.

In other experiments [12], spectra of proton kinetic energies, produced during the photoionization of the molecular ion, were accumulated. These spectra showed a tendency of protons to appear with kinetic energies peaked slightly below 1.5 eV, for laser conditions similar to those which we have chosen. However, from Fig. 5 we can see that our simulations exhibit a peak at significantly higher energies; i.e., just below 2.5 eV. To emphasize this point, we include in Fig. 16 the data from Figs. 2 and 5, summed over angle and plotted as a function of fragment kinetic energy.

Recently published experimental data describing the breakup of H_2 [14] are consistent with our simulations. In particular, fragmentation spectra accumulated for the dissociative ionization and the double photoionization regimes show close similarity with our results; compare our Fig. 17 with Fig. 2 of Ref. [14]. The so-called 1ω and 2ω peaks are evident in both cases, as is the so-called charge resonance enhanced ioinization (CREI) peak at approximately 3 eV, for double photoionization. The NSDI region of double photoionization, for energies greater than 4.5 eV also appears in both cases. However, for circular polarization there are no final states with proton kinetic energies greater than approximately 4.5 eV [14,23]; see Fig. 18. Finally, there is also evi-

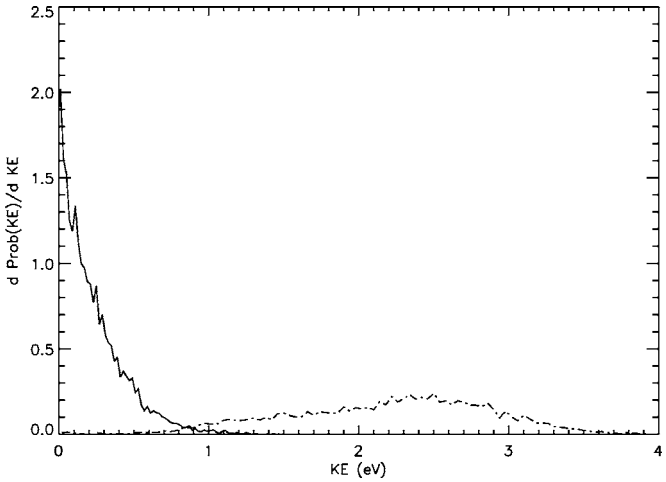

FIG. 16. For the breakup of H_2^+: distribution of fragment kinetic energies (summed over Θ), for the conditions of Fig. 2; photodissociation (solid curve); photoionization (dash-dot curve); see text.

dence for the appearance of a triple peak structure in the CREI region, in both cases; compare our Fig. 17 with Fig. 8 of Ref. [14].

We note that an earlier published conjecture regarding the breakup of H_2 [24] is inconsistent with the results of our simulations; viz., we have found no evidence for the existence of a molecular ion intermediate in the fragmentation of H_2. Rather, it appears that a transient dissociative state usually precedes the more complete breakup of H_2; i.e., for the laser conditions which we picked, and according to FMD. Of equal importance, a 2H final state apppears with a significant probability in our simulations.

Admittedly, there is no existing experimental evidence for the production of a purely dissociated (2H) state during the breakup of H_2 [14,15] for the laser conditions of interest here. Nevertheless, at least some laboratory measurements

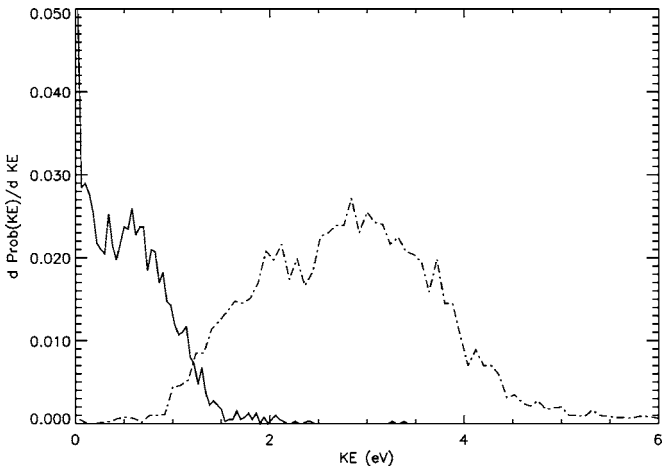

FIG. 17. For the breakup of H_2: distribution of fragment kinetic energies (summed over Θ), for the conditions of Fig. 10; photodissociative ionization (solid curve); double photoionization (dash-dot curve); see text. As with all of the data presented in this paper, up to this point, this is for laser *linear* polarization; see Fig. 18 for circular polarization.

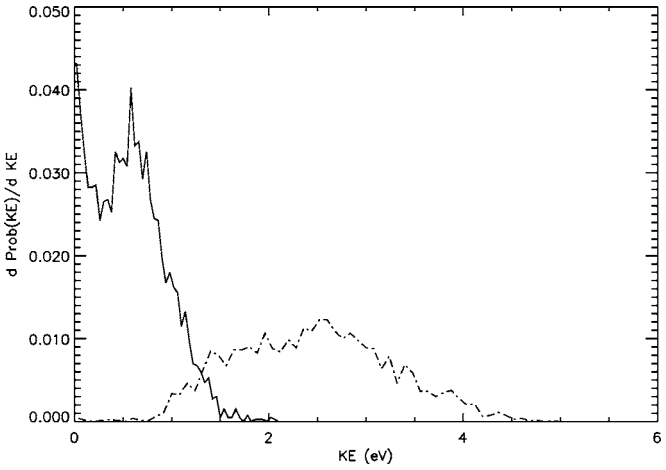

FIG. 18. For the breakup of H_2: distribution of fragment kinetic energies (summed over Θ), for a *circularly* polarized laser with $E_0=0.039$ a.u. ($I_0=1.06\times10^{14}$ W/cm^2), $\omega=0.060$ a.u. ($\lambda=758$ nm), and $t_{pulse}=4300$ a.u. (100 fs); photodissociative ionization (solid curve); double photoionization (dash-dot curve); compare with Fig. 17.

seem to suggest that the molecular ion is not the sole antecedent to further breakup of H_2; see Fig. 1 of Ref. [15].

Finally, we would like to expand a bit more upon one of the previously mentioned limitations of FMD. Namely, we recall that there is a continuum of low-lying excited states accessible to all bound electronic systems, in the present formulation of FMD. Therefore, in spite of the fact that ground electronic states can always be well-described by FMD, the description of transitions which pass through bound electronic excited intermediate states is problematic. In our case, this defect is expected to have affected details of the description of transitions out of the ground states of H_2^+, and H_2. Consequently, conclusions about fragmentation mechanisms deduced from the present formulation of FMD are uncertain.

We say this in spite of the fact that there is usually an increase in the number of distinct low-lying bound electronic states made accessible to the outermost electron, in a multielectron atom or ion, due to electron-electron correlation [8]. Such an increase might conceivably lead to a system more amenable to treatment by quasiclassical methods; e.g., for H_2, although not for H_2^+.

We consider specific examples of this phenomenon, occurring for ionic (uninuclear) systems: For a single $n=2$ excited electron in a hydrogenlike ion there is only one distinct state (of multiplicity 8). However, for two $n=2$ electrons in a heliumlike ion there are six clustered, and generally nonoverlapping, discrete states: $2s^2(^1S_0)$, $2s2p(^1P_1,^3P_1)$, and $2p^2(^1S_0,^3P_1,^1D_2)$. Unfortunately, these states will also usually be doubly excited states. The situation for two-electron singly excited states is less advantageous since there are only four such distinct $1s2\ell$ states.

Improvements may occur for larger systems, with open-shell ground states. For instance, for a nitrogenlike ion with just one $n=3$ electron there are 26, generally nonoverlapping, discrete singly excited states: $1s^22s^22p^2$ ($^1S_03\ell$, $^3P_13\ell$, and $^1D_23\ell$), where the first term in parenthesis contains three doublet states, the second term seven doublet states and

seven quartets, and the third term nine doublets. However, in this case there are also many low-lying excitations contained within the ground state configuration itself, and this would appear to complicate the application of any quasiclassical approach. More fundamentally, the cluster of lowest lying single excited states remains well-separated from the cluster of "ground states."

Thus we say that the presence of a wide gap between the ground state, or states, and the first excited state, or states, in the spectrum of most Coulombic systems remains a significant problem for general applications of the FMD method, as presently formulated. A special case, worth pointing out, does allow for a reduction in the seriousness of this defect. Namely, if the laser pulse length can be made short enough, then the uncertainty principle will come into play. For example, if $t_{pulse} < 0.3$ fs, then a broadening of otherwise discrete energy levels occurs, according to $\Delta\epsilon \geqslant 2\pi/t_{pulse} \sim 14$ eV. This leads to a "merging" of the ground and first excited states of H; and, indeed, an overlapping of all of the otherwise discrete states.

This generally serious problem with FMD notwithstanding, it should go without saying that full quantum calculations, for multielectron time dependent systems, have many of their own limitations. For example, although explicit coupling between the electronic ground state and the electronic component of the discrete lowest-lying dissociating state of a diatomic molecule is almost always featured in such calculations, description of the coupling to more highly excited electronic states, and of the molecular breakup process itself is almost always incomplete.

Therefore it appears that a way forward into the future might be to perform mixed quantum and FMD calculations. In such a formulation, each of the ground electronic states in the problem, and its coupling to the corresponding lowest-lying excited electronic state, or states, would be treated by means of the time-dependent Schrodinger equation. For the H_2 and H_2^+ systems, this coupling would occur at a fixed value of the internuclear coordinate R, and would be to the corresponding lowest-lying dissociating state. Simultaneously, coupling of these lowest-lying discrete electronic excited states to other more highly excited electronic states, and to the corresponding electronic continua, and the propagation of the coordinates and momenta of both protons, would be performed by FMD. It is expected that the description of transitions between closely spaced highly excited electronic states are well-described by FMD; i.e., for both bound highly excited states and for continua. This formulation would also help to realize more general recent proposals for mixed quantum and classical calculations [25].

ACKNOWLEDGMENTS

The development of the FMD method, for application to problems in atomic and molecular physics, owes much to the efforts of J. S. Cohen. The author thanks Dr. Cohen for his many helpful comments and suggestions as this paper was being prepared.

APPENDIX

We will derive the values of the threshold electric field strengths for over-the-barrier ionization of the ground states of: (1) atomic hydrogen; (2) the hydrogen molecular ion; and (3) molecular hydrogen. We will work entirely in one dimension, and use only classical arguments.

1. H: The potential seen by the bound electron may be written as

$$V(x) = -1/x - xE \tag{A1}$$

for $x > 0$, and where E is the laser (peak) electric field strength, for linear polarization. This function has a maximum at a value of x given by the solution of

$$\partial V(x)/\partial x = 1/x^2 - E = 0 \tag{A2}$$

from which we obtain the relationship

$$x_{OBI} = 1/\sqrt{E_{OBI}}. \tag{A3}$$

Since the total energy of the bound electron is $E_{TOT} = -0.5/n^2$ a.u., where n is the principal quantum number ($n = 1$ for the g.s.), then the electron just escapes the potential well (escapes with zero velocity) if

$$E_{TOT} = V(x_{OBI}). \tag{A4}$$

This establishes the threshold electric field strength as

$$E_{OBI} = 1/16n^4 \text{ a.u.} \tag{A5}$$

and

$$x_{OBI} = 4n^2 \text{ a.u.} \tag{A6}$$

For g.s. hydrogen, this threshold field strength is $E_{OBI} = 0.0625$ a.u.

2. H_2^+: The potential seen by the bound electron is two-centered. Repeating the procedure in (1),

$$V(x) = -1/|x - R/2| - 1/|x + R/2| - xE, \tag{A7}$$

where R is the internuclear separation. This function has a maximum for an x such that $\partial V(x)/\partial x = 0$. After some algebra, one finds the following relationship between x_{OBI} and E_{OBI}:

$$x_{OBI} = \sqrt{R^2/4 + 1/E_{OBI} + [(1/E_{OBI})(1/E_{OBI} + R^2)]^{1/2}}. \tag{A8}$$

We take the total energy of H_2^+ to be $E_{TOT} = -0.6027$ a.u. Setting this number equal to the value of the potential, at its maximum, one arrives at a second equation relating x_{OBI} to E_{OBI}, to be solved simultaneously with the first:

$$0.6027 = x_{OBI}[8/(4x_{OBI}^2 - R^2) + E_{OBI}]. \tag{A9}$$

Putting in the value of the internuclear separation as $R = 2.32$ a.u. one then arrives at the solution of the coupled equations as

$$x_{OBI} = 7.0 \text{ a.u.} \tag{A10}$$

and

$$E_{OBI} = 0.044 \text{ a.u.} \tag{A11}$$

If internuclear motion is included, then the total energy increases. For example, at a temperature of 2300 K, the total

energy increases to $E_{TOT}=-0.596$ a.u., so that $x_{OBI}=7.1$ a.u. and $E_{OBI}=0.043$ a.u.

From a dissociating state, as R increases the total system energy, as well as the values of E_{OBI} and x_{OBI}, all change. For example, at $R=3.8$ a.u. one has that $E_{OBI}=0.036$ a.u. and $x_{OBI}=8.1$ a.u.; whereas, for $R=5.9$ a.u. one finds $E_{OBI}=0.030$ a.u. and $x_{OBI}=9.5$ a.u.

3. H_2: There is a second electron, which remains bound. We denote the coordinate of this electron by x_0, where $0 \leqslant x_0 < R/2$ is fixed. We also assume that R is fixed at its equilibrium value; i.e., $R=1.40$ a.u. for H_2, and take the binding energy of the first electron to be $E_{TOT}=-0.599$ a.u., which is the energy difference between the ground electronic states of H_2 and H_2^+, at $R=1.40$ a.u. Equations (A1) and (A2) are now altered to reflect the presence of the second electron, and depend explicitly upon x_0.

For example, from the analogs of Eqs. (A1) and (A2), and for the assumed value $x_0=0$, we find that $x_{OBI}=3.81$ a.u. and $E_{OBI}=0.084$ a.u. If instead, we allow to second electron to be displaced to the right, and such that $x_0=R/2$, then we obtain $x_{OBI}=3.89$ a.u. and $E_{OBI}=0.066$ a.u. Of course, generally, the second electron is in rapid motion and not confined to any one location. Consequently, this last result is only suggestive.

In the preceding, we have ignored questions adiabaticity relating to the turning on of the laser pulse. These questions, when addressed, may change our computed values of E_{OBI} [26].

[1] K. LaGattuta, J. Opt. Soc. Am. B **7**, 639 (1990); K. LaGattuta, Phys. Rev. A **43**, 5157 (1991).
[2] J. S. Cohen, Phys. Rev. A **57**, 4964 (1998).
[3] B. Feuerstein and U. Thumm, Phys. Rev. A **67**, 043405 (2003).
[4] S. Chelkowski, C. Foisy, and A. D. Bandrauk, Phys. Rev. A **57**, 1176 (1998).
[5] K. LaGattuta and J. S. Cohen, J. Phys. B **31**, 5281 (1998).
[6] P. B. Corkum, Phys. Rev. Lett. **71**, 1994 (1993).
[7] K. LaGattuta, J. Phys. B **33**, 2489 (2000).
[8] P. J. Ho and J. H. Eberly, Phys. Rev. Lett. **95**, 193002 (2005); P. J. Ho, R. Panfili, S. L. Haan, and J. H. Eberly, *ibid.* **94**, 093002 (2005).
[9] C. Ruiz, L. Plaja, L. Roso, and A. Becker, Phys. Rev. Lett. **96**, 053001 (2006).
[10] J. Chen and C. H. Nam, Phys. Rev. A **66**, 053415 (2002); L. B. Fu, J. Liu, and S. G. Chen, *ibid.* **65**, 021406R (2002).
[11] K. Sandig, H. Figger, and T. W. Hansch, Phys. Rev. Lett. **85**, 4876 (2000).
[12] D. Pavicic, A. Kiess, T. W. Hansch, and H. Figger, Phys. Rev. Lett. **94**, 163002 (2005).
[13] I. Ben-Itzhak, P.Q. Wang, J. F. Xia, A. M. Sayler, M. A. Smith, K. D. Carnes, and B. D. Esry, Phys. Rev. Lett. **95**, 073002 (2005).
[14] A. Rudenko *et al.*, J. Phys. B **38**, 487 (2005).
[15] H. Rottke *et al.*, Phys. Rev. Lett. **89**, 013001 (2002).
[16] D. Zeidler, A. Staudte, A. B. Bardon, D. M. Villeneuve, R. Dorner, and P. B. Corkum, Phys. Rev. Lett. **95**, 203003 (2005).
[17] J. S. Cohen, Phys. Rev. A **56**, 3583 (1997).
[18] D. Bohm, Phys. Rev. **85**, 166 (1952).
[19] C. L. Kirschbaum and L. Wilets, Phys. Rev. A **21**, 834 (1980).
[20] J. S. Cohen, Phys. Rev. A **51**, 266 (1995); **57**, 4964 (1998).
[21] K. LaGattuta, Workshop on Currents and Trajectories in Quantum Mechanics, CECAM, Lyon, France, 2002 (unpublished).
[22] J. S. Cohen, J. Phys. B **37**, 525 (2004).
[23] H. Sakai, J. J. Larsen, I. Wendt-Larsen, J. Olesen, P. B. Corkum, and H. Stapelfeldt, Phys. Rev. A **67**, 063404 (2003).
[24] P. H. Bucksbaum, A. Zavriyev, H. G. Muller, and D. W. Schumacher, Phys. Rev. Lett. **64**, 1883 (1990).
[25] K. LaGattuta, J. Phys. A **36**, 6013 (2003).
[26] J. S. Cohen, Phys. Rev. A **64**, 043412(R) (2001).